On the morphology of a discotic liquid crystalline charge transfer complex

Haverkate, L.A.; Zbiri, M.; Johnson, M.R.; Deme, B.; Groot, H.J.M. de; Lefeber, A.W.M.; ... ; Kearley, G.J.

On the Morphology of a Discotic Liquid Crystalline Charge Transfer Complex

Lucas A. Haverkate,[†] Mohamed Zbiri,[‡] Mark R. Johnson,[‡] Bruno Deme,[‡] Huub J. M. de Groot,[||] Fons Lefeber,[||] Arkadiusz Kotlewski,[⊥] Stephen J. Picken,[⊥] Fokko M. Mulder,*,[†] and Gordon J. Kearley[§]

[†]RID, Faculty of Applied Sciences, Delft University of Technology, Mekelweg 15, 2629JB Delft, The Netherlands
[‡]Institut Laue Langevin, 38042 Grenoble Cedex 9, France
[§]Bragg Institute, Australian Nuclear Science and Technology Organisation, Menai, NSW 2234, Australia
[||]Biophysical Org. Chemistry Solid State NMR, Leiden University, LIC, NL-2333 CC Leiden, Netherlands
[⊥]ChemE-NSM, Faculty of Chemistry, Delft University of Technology, 2628BL/136 Delft, The Netherlands

S *Supporting Information*

ABSTRACT: Discotic liquid crystalline (DLC) charge transfer (CT) complexes, which combine visible light absorption with rapid charge transfer characteristics within the CT complex, can have a great potential for photovoltaic applications when they can be made to self-assemble in a bulk heterojunction arrangement with separate channels for electron and hole conduction. However, the morphology of some liquid crystalline CT complexes has been under debate for many years. In particular, the liquid crystalline CT complex built from the electron acceptor 2,4,7-trinitro-9-fluorenone (TNF) and discotic molecules has been reported to have the TNF "sandwiched" either between the discotic molecules within the same column or between the columns within the aliphatic tails of the discotic molecules. We present a detailed structural study of the prototypic 1:1 mixture of the discotic 2,3,6,7,10,11-hexakis(hexyloxy)triphenylene (HAT6) and TNF. Nuclear magnetic resonance (NMR) line widths and cross-polarization rates are consistent with the picosecond time scale anisotropic thermal motions of the HAT6 and TNF molecules previously observed. By computational integration of Rietveld refinement analyses of neutron diffraction patterns with density experiments and short-range structural constraints from heteronuclear 2D NMR, we determine that the TNF molecules are vertically oriented between HAT6 columns. The data provide the insight that a morphology of separate hole conducting channels of HAT6 molecules can be realized in the liquid crystalline CT complex.

Bottleneck: no electron channel

Hole transport
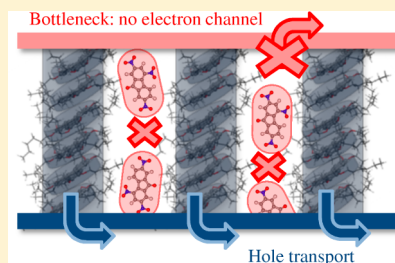
INTRODUCTION

In recent years, discotic liquid crystals (DLCs) have become a promising class of organic materials for photovoltaic and other electronic applications.[1−6] These disk-like molecules form stable columns due to the overlap of the π-orbitals of their aromatic core and tail−tail interactions, while thermal fluctuations of their side chains (tails) give rise to the liquid-like dynamic disorder. Like conjugated polymers,[7−10] DLCs could be used as low cost, easily processed, and flexible solar cells. Further, DLCs exhibit advantageous properties including visible light absorption, long-range self-assembly, self-healing mechanisms, high charge-carrier mobilities along the column axis, and a tunable alignment of the columns.[1,5,11] It is generally thought that optimal performance of DLC solar cells is most effectively achieved within a bulk heterojunction (BHJ) setup, with separate channels for electron and hole transport, and the donor and acceptor materials intermixed at a length scale less than the exciton diffusion length.[4,6,7,10]

An interesting design route to achieve such a device architecture is to dilute the columnar liquid crystalline phase with a nondiscogenic electron acceptor, such as 2,4,7-trinitro-9-fluorenone (TNF).[6,11−13] Although pure DLCs generally show a poor absorption in the visible spectral domain, mixtures of the

electron-donating discoids with nondiscogenic electron acceptors could exhibit absorption bands in the visible due to the formation of a charge transfer (CT) complex.[14−16] In many cases CT complexation even causes a considerable increase in the stability of the columnar mesophase.[17,18] Despite these favorable properties, it is still unclear to what extent DLC-CT compounds can be attractive for application in a photovoltaic device. For good performance of a photovoltaic device the donor and acceptor molecules must form separate columns, i.e., enable charge separation and subsequent charge transport along the columnar wires. The position of the electron acceptors within the columnar mesophases is still controversial.[13] Acceptor molecules such as TNF have been reported to be "sandwiched" between discotic molecules within the same column[14,19−21] but also "intercolumnar", i.e., between the columns within the aliphatic tails of the discotic molecules.[17,22−25] Only the intercolumnar juxtaposition could provide a morphology with separate continuous columns for electron and hole transport.[17] Another issue is that the

characterization of (photoinduced) electron transfer and relaxation processes in self-assembled aggregates such as DLCs and DLC-CTs is in its infancy.[26] The addition of electron acceptors such as TNF has been shown to increase the conductivity of DLCs.[12,23,27,28] On the other hand, it has been proposed that recombination processes limit the hole photo-current in DLC-CT compounds.[29] Charge carriers in CT compounds are supposed to be trapped and readily annihilated through rapid, phonon-assisted relaxation and recombination processes.[3,29,30]

Here we elucidate the morphology issue by considering a prototypical discotic CT compound. We used the widely discussed hexakis(n-hexyloxy)triphenylene (HAT6)[31] as electron-donating discoid and TNF as electron acceptor (Figure 1).
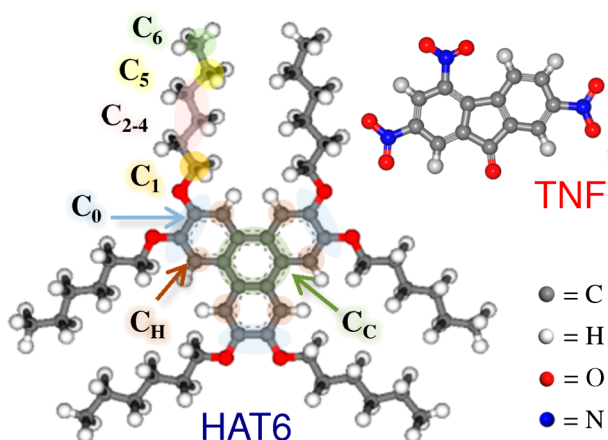

Figure 1. Illustration of HAT6 (D_{3h} symmetry) and TNF, including the labeling of the HAT6 carbons used for the NMR analysis.

The resulting 1:1 mixture HAT6-TNF forms a CT compound exhibiting a stable liquid crystalline columnar phase from below room temperature to 237 °C.[17] For a detailed examination of the morphology, the sandwich and intercolumnar juxtaposition were compared directly by a combined analysis of neutron diffraction, nuclear magnetic resonance (NMR), and mass density experiments. In addition, the possibility of ground state charge transfer is discussed by analyzing the chemical shifts in the NMR spectra.

■ MATERIALS AND METHODS

Sample Preparation. Isotopically normal 2,3,6,7,10,11-hexakis(hexyloxy)triphenylene (HAT6) and its side-chain deuterated analogue, HAT6d, were prepared by the synthesis methods described earlier.[17,32] The charge transfer compounds were obtained by mixing HAT6 (or HAT6d) with 2,4,7-trinitro-9-fluorenone (TNF) in a 1:1 molar proportion in dichloromethane.[17] The mixture was subsequently evaporated to dryness at room temperature. To remove any traces of solvent and to ensure the correct phase behavior, the resulting composite was heated to the isotropization temperature, 237 °C, and then cooled slowly. By using a deuterated analogue for TNF as well (TNFd, with all hydrogens deuterated), four analogues were obtained: HAT6-TNF, HAT6d-TNF, HAT6-TNFd, and HAT6d-TNFd. The degree of deuteration of HAT6d and TNFd was about 98 atom %.

Density Measurements. Helium pycnometry was used for accurate density measurements of HAT6-TNF in the liquid crystalline phase. Helium is inert and can penetrate into voids smaller than 0.4 nm, enabling the skeletal density to be measured without voids. We used a Quantachrome Pentapycnometer to measure the skeletal volume of 1.267 g of the fully deuterated sample HAT6d-TNFd. The skeletal volume over 10 measurements at 300 K was 1.17 cm^3 ± 1%.

Neutron Powder Diffraction. Neutron powder diffraction of HAT6-TNF and its deuterated analogues was performed using the D16 diffractometer at the Institut Laue Langevin (ILL) in France. A wavelength of 4.54 Å was selected to provide a good compromise between d-spacing range and angular resolution. The advantage of using neutron diffraction is that the neutron scattering cross section is determined by the nucleus only; i.e., there is a constant atomic form factor, which leads to larger diffraction intensity for an extended d-spacing range and information related to the thermal motions (temperature factors). In addition, the cross section is of different sign for protons and deuterium. As a consequence, the neutron powder diffraction pattern of the tail-deuterated sample HAT6D an HAT6D-TNF provide e.g. larger d-spacing range information about the deuterated part of the structure than X-ray powder diffraction experiments can provide.[17] By using the selectively deuterated samples, we were able to tune the amount of diffraction from different molecular regions, due to the large difference between the neutron scattering cross sections of hydrogen and deuterium.

Rietveld Refinement. An important step in our approach is a direct comparison of the neutron powder diffraction patterns with model structures representing the different juxtapositions of TNF. Unlike in our earlier work on pure HAT6,[31,33] this required a full Rietveld refinement procedure to bridge the gap between initial model and final structure. The refinement was performed using the Reflex package as incorporated in the Materials Studio suite 4.2, which is capable of refining crystal structures with more than 500 atoms in the unit cell. For large structures, such as those considered here, refinement is only possible if constraints are made to the large parameter space. Therefore, we incorporated two main types of constraints in the refinement procedure. First, the molecular degrees of freedom were limited by treating the HAT6 and TNF molecules as rigid bodies during refinement. For TNF (28 atoms) this resulted in a reduction of the parameter space to three translational and three rotational degrees of freedom per molecule. For HAT6 (144 atoms) we also incorporated the first three dihedral angles of the HAT6 tails (C_0−O, O−C_1, and C_1−C_2 in Figure 1), giving rise to 18 additional refinement parameters per HAT6 molecule. Second, an energy penalty term was included during refinement to reduce the solution space to structures that are energetically feasible, i.e., without unrealistic molecular and atomic distances. We optimized the combined figure of merit $R_{comb} = (1 − w)R_{wp} + wR_E$ as implemented in Reflex, with R_{wp} being the measure of agreement between observed and calculated diffraction patterns. The energetic contribution $R_E = 0.1(E − E_{min})/E_{tol}$ ensures that the potential energy E of realistic solutions should be within a given tolerance E_{tol} (= 40 kcal/mol in the present case) of the global energy minimum E_{min}. We have set the energetic weight factor w to 0.01. Using such a small value *de facto* means that R_E is mainly used to guide the optimization out of unfavorably high energy regions with for instance atomic overlaps or unrealistic intermolecular distances. The potential energies were calculated before (E_{min}) and during (E) Rietveld refinement using the COMPASS force field.[34−36] Coulomb and van der Waals interactions were summed using the atomistic approach,[37] and the Lennard-Jones

function was truncated at a cutoff distance of 10 Å. A spline width of 1 Å was chosen in order to turn off the nonbond interactions smoothly. A long-range correction for the effects of splining and cutoff was applied in the standard way.[38] The atomic charges were assigned using the values provided by the COMPASS force field.

Model Structures. The cell parameters of the initial model structures were estimated from the observed column−column reflections ([100], [010]) and intracolumnar nearest-neighbor spacing [001] (see Figure 1), together with the constraint imposed by the measured density of HAT6-TNF. The sandwich structure was built by constructing a 2 × 2 × 4 supercell of 8 HAT6 and 8 TNF molecules, allowing an alternate packing of HAT6 and TNF both along and perpendicular to the column director. For the intercolumnar model we used a 2 × 2 × 3 supercell consisting of 4 columns of 3 HAT6 molecules, with 12 vertically oriented TNF molecules evenly distributed between the tails. The initial molecular conformations of HAT6 and TNF were preoptimized using the COMPASS force field, with a fixed D_{3h} molecular symmetry for HAT6, with the tail torsions being all-trans (Figure 1). For both the sandwich and intercolumnar juxtaposition of TNF we have tested other supercell structures, but they all faced fundamental packing problems and/or a bad agreement with the experimental diffraction patterns.

Solid State CP-MAS NMR. Solid state ^{13}C CP-MAS and 2D heteronuclear ($^1H-^{13}C$) correlation spectra were recorded using a DMX-400 (9.4 T) NMR spectrometer operating at a ^{13}C frequency of 100.5 MHz, equipped with a 4 mm triple-resonance CP/MAS probe (Bruker, Karlsruhe, Germany). To minimize unwanted spectral overlap, the MAS spinning frequency was set at 8 kHz, unless quoted otherwise. During all experiments the spinning frequency was kept stable to within a few hertz. The spectra were obtained with cross-polarization (CP) mixing times between 100 μs and 10 ms. The $^1H-^{13}C$ 2D heteronuclear correlation spectra were obtained using the CP/WISE technique as described elsewhere.[39] Following a 90° pulse on the protons, a time increment (t_1) before the CP allows the proton evolution to be observed with detection through the carbons. A ramped amplitude CP sequence (RAMP-CP) was implemented to restore a broader Hart-mann−Hahn matching profile.[40] During the t_2 evolution time, the protons were decoupled from the carbons by using the two-pulse phase-modulation (TPPM) decoupling scheme.[41] The 90° proton pulse lengths were typically between 3 and 4 μs. The 2D spectra were recorded with 64 points in the t_1 (^1H) and 1510 points in the t_2 (^{13}C) dimension.

■ RESULTS

Neutron Diffraction. The neutron diffraction pattern of HAT6-TNF (Figure 2) is characteristic for a columnar mesophase, with sharp reflections in the small 2Θ region ([100], [010], etc.) originating from the 2D columnar lattice, a broad liquid-like band from the distribution in tail−tail distances, and a broad [001] peak from the intracolumnar distances.[31] The Bragg peak from the distance between the columns is shifted from 1.85 nm for HAT6 to 1.53 nm for HAT6-TNF. Also, the intracolumnar peak, reflecting the characteristic cofacial nearest-neighbor distance, is shifted, from 3.65 to 3.40 Å. Two observations are important here. First, there is no superstructure peak visible with a double cofacial distance as would result in a intracolumnar juxtaposition of TNF where TNF and HAT6 alternate,
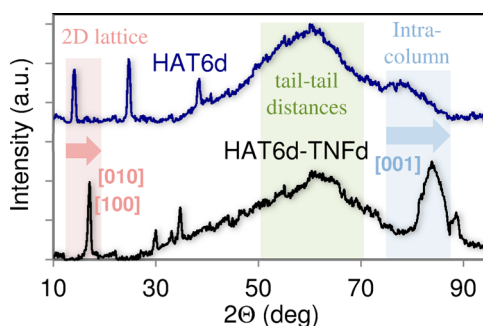

Figure 2. Neutron diffraction patterns of HAT6d at 345 K (top) and HAT6d-TNFd at 300 K (bottom). The arrows indicate the changes in the [100]/[010] intercolumnar and [001] intracolumnar distances.

doubling the cell dimensions in the z-direction. This essentially makes such configurations unlikely. Second, the large decrease in lattice parameters is not accompanied by a similar increase in density that would result when simply shrinking the HAT6 cell to the new dimensions. We measured a skeletal density of 1.08 ± 0.01 g cm^{-3} for HAT6d-TNFd, corresponding to an increase in density of about 7% with respect to HAT6.[17] These observations indicate that the columnar morphology has drastically changed in the charge transfer compound. For a hexagonal columnar structure with the TNF sandwiched between the HAT6 molecules, the column−column distance should be about 17% smaller compared to pure HAT6. This only appears possible if the HAT6 and TNF are also alternately packed in the hexagonal plane. Other distributions result in energetically unfavorable interdigitation of the aliphatic tails, such as the often suggested[42] alternating intracolumnar packing with the discotic molecules positioned in the same hexagonal plane. The intracolumnar juxtaposition of TNF, on the other hand, is only consistent with the experiments if the HAT6 columns are tilted on an oblique lattice. Such an arrangement, with discotic molecules slid laterally, has already been observed for highly polar HAT2-NO$_2$ molecules.[43] However, the tilted HAT6 columns leave such small spaces within the tail region that the TNF molecules should mainly have a vertical orientation.

The sandwich (with HAT6 and TNF alternating in the horizontal plane) and intracolumnar (with tilted HAT6) models were further analyzed with Rietveld refinement. Figure 3 compares the calculated intensities with experimental data, while the assignment of the main reflections from the 2D columnar lattice is shown in Figure S9 for both supercell models. Remarkably, the refinement does not favor either of the juxtapositions of TNF over the other. Both models reproduce the characteristic features of the experimental diffraction patterns with comparable agreement, and both morphologies are also energetically reasonable with fair agreement with the observed macroscopic density (Table 1). In addition, the effect of deuteration on the diffraction patterns also fits well with the measurements in both cases, particularly considering that no extra refinement step has been made from Figure 3b to Figure 3a; i.e., only the deuterium atoms of TNF were replaced with protons. Even the orientation dependences of the diffraction patterns on macroscopically aligned samples show little difference between the two models (see Supporting Information). As expected, the 2D lattice peaks have maximum intensity when the diffraction beam is perpendicular to the column director, and the intracolumnar peak is at a maximum
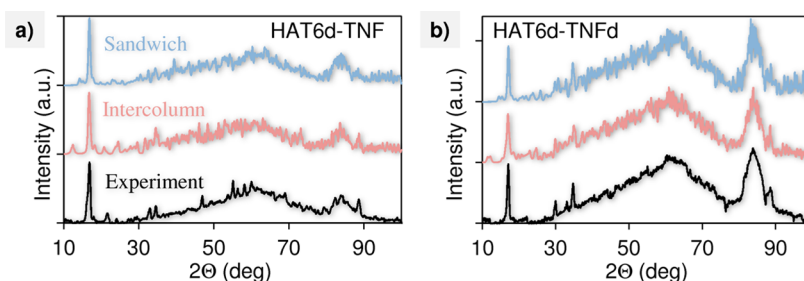
Figure 3. Comparison between the neutron diffraction patterns of the refined sandwich (top) and intercolumnar (center) models and the measurements at 300 K (bottom) for (a) HAT6d-TNF and (b) HAT6d-TNFd.

Table 1. Structural Properties Extracted from the Refined Models

	sandwich	intercolumn
density^a (g cm^{-3})	1.14	1.10
a^b (nm)	3.39	5.02
b^b (nm)	3.43	5.04
c^b (Å)	13.76	14.97
α (deg)	83.4	64.8
β (deg)	92.4	72.9
γ (deg)	116.3	120.7
$d_{column-column}$ (nm)	~1.8	~2.2
$d_{core-core}$ (Å)	3.42	3.40
$d_{HAT6core-TNF}^c$ (Å)	~3.4	4–10^d
columnar slide (Å)	~0.4	~3.5

^{a}Density of the deuterated samples HAT6d–TNFd. ^{b}Lattice parameters of the 2 × 2 × 4 sandwich and 2 × 2 × 3 intercolumn supercells. ^{c}Shortest distance between the core of HAT6 and TNF. ^{d}Estimate of different TNF orientations that were refined.

for the parallel orientation. Clearly, it is difficult to determine the juxtaposition of TNF using only diffraction. Nevertheless, the sandwich and intercolumnar models only fit with the observed density and diffraction patterns under the conditions given in Table 1 and illustrated in Figure 4. As anticipated, the HAT6 columns in the intercolumnar model are tilted, with a cofacial slide of about 3.5 Å between two neighboring molecules in a column. We defined $d_{column-column}$ as the average separation between the column directors (Figure 4) of two neighboring columns, which is significantly larger for the
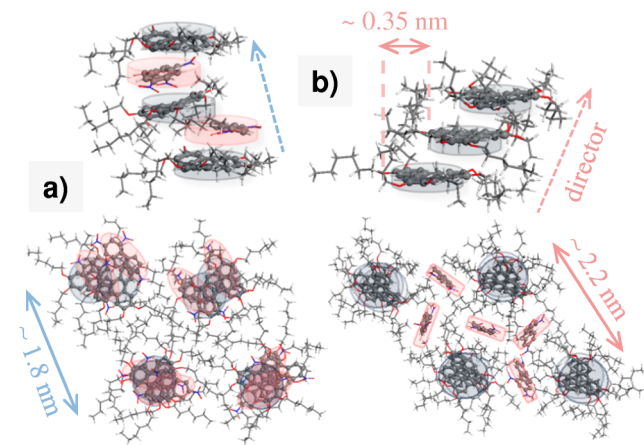

Figure 4. Illustration of (a) the sandwich and (b) the intracolumnar model structures after Rietveld refinement. Elliptical pink shape: TNF; gray disk: HAT6.

intercolumn juxtaposition of TNF. The minimal distance $d_{HAT6core-TNF}$ between the core of HAT6 and TNF predominantly determines the charge-transfer behavior of the complex. For the intercolumnar arrangement $d_{HAT6core-TNF}$ is difficult to estimate, since there is considerable freedom left in the refinement of the TNF position. We refined several intercolumn models with different initial vertical positions of TNF from which we estimated that $d_{HAT6core-TNF}$ should be within the range of 4−10 Å. Typically, the closest distance between TNF and HAT6 for the intracolumnar juxtaposition involved a C_H carbon of HAT6 and a NO_2 group of TNF.

Solid State NMR. Figure 5 shows the solid state ^{13}C CP MAS NMR spectra of liquid-crystalline HAT6, TNF, and the
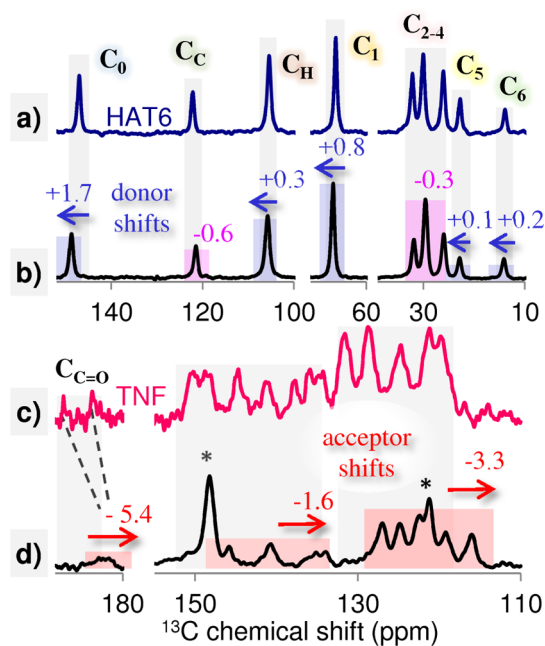

Figure 5. Solid state CP-MAS ^{13}C NMR spectra for HAT6 (a), HAT6-TNFd (b), TNF (c), and HAT6-TNF (d). The temperature and CP mixing time are 358 K, 10 ms for (a, b), 300 K, 2 ms for (c), and 300 K, 5 ms for (d). The HAT6 carbon assignment in (a) follows the labeling of Figure 1. The blue (red) arrows indicate the downfield (upfield) shifts of HAT6 (TNF) peaks in the composite.

CT complex. An overview of the assignment of these spectra can be found in the Supporting Information. Solid state ^{13}C, ^{1}H, and ^{2}H NMR spectra have already been reported for protonated and side-chain deuterated triphenylene-based DLCs,[44−47] and the analysis of the carbon signals of HAT6 presented in Figure 5a is in line with this literature. The assignment of TNF has also been performed earlier.[48,49] On the
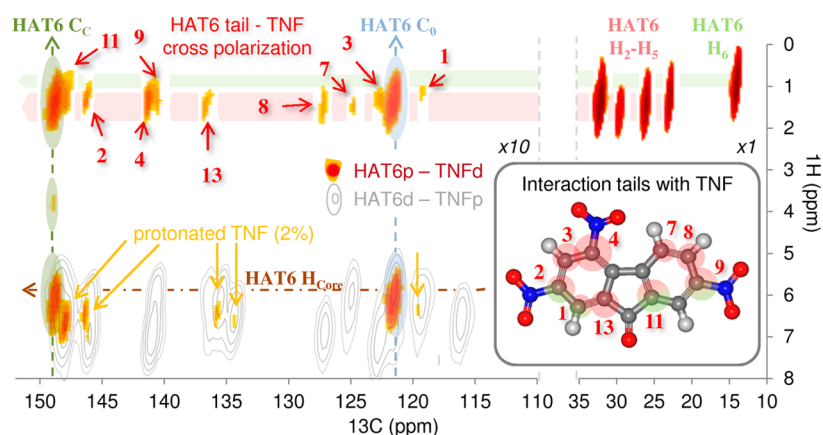
13101

dx.doi.org/10.1021/jp306412u | J. Phys. Chem. B 2012, 116, 13098−13105

Figure 6. $^1\text{H}-^{13}\text{C}$ 2D heteronuclear correlation spectra for HAT6-TNFd (colored contours) and HAT6d-TNF (gray contours) at 290 K with a CP mixing time of 10 ms. The red numbers indicate cross-polarization between protons on the tail of HAT6 (H_2-H_5 and H_6) and specific TNF carbons shown in the inset. The circles in the inset surrounding the numbered carbons illustrate the strength of these interactions and the possible HAT6 hydrogens involved (pink for H_2-H_5, green for H_6). The HAT6 C_c and C_0 carbon and the H_{core} hydrogen chemical shifts are indicated by the green, blue, and brown dashed lines, respectively. The signals marked with yellow arrows are due to imperfect deuteration of TNF.

basis of these spectra of the uncomplexed samples, we assigned all the peaks in the CT-complex spectrum to specific HAT6 or TNF carbons (Figures S3 and S5). In the CT compounds, however, the chemical shifts of the HAT6 and TNF carbons are changed significantly. All the TNF carbon signals are shifted upfield (Figure 5d and Table S1), reflecting a stronger local magnetic field for the TNF in the mixture compared with the pure compound. The largest shift of −5.4 ppm is observed for the C=O carbon C_{12}, and the signals of the C_5 and C_6 in the central 5-ring moderately shift upfield by −0.7 and −0.2 ppm, respectively. In contrast to TNF, the HAT6 lines show both downfield and upfield shifts, with a net downfield shift of 9.6 ± 0.2 ppm summed over the whole molecule. The strongest downfield shifts are observed for outer carbons of the aromatic core, C_0 (1.7 ppm) and C_H (0.3 ppm), and the first tail carbon C_1 (0.8 ppm).

Chemical shift changes in charge transfer complexes have been attributed to partial electron transfer from donor to acceptor molecules in the electronic ground state.[15,49,50] According to Mulliken's theory,[16] partial transfer of electron density occurs from the highest occupied molecular orbital (HOMO) of the donor to the lowest unoccupied molecular orbital (LUMO) of the acceptor in the electronic ground state. Indeed, for the HAT6 donor we observe the anticipated general shift sign (lower electron density, lower field) that would result from partial electron transfer to the acceptor TNF. For HAT6 the largest downfield shifts are observed for ^{13}C nuclei in the outer part of the aromatic core, which is consistent with the spatial distribution of the HOMO.[51,52] However, the observed shifts could correspond to a small amount of intermolecular electron transfer in the ground state of HAT6-TNF. To a first approximation, a unit positive charge on a single carbon induces a downfield shift of about 160 ppm.[15] The net downfield shift of 9.6 ppm on HAT6 would then correspond to a total ground-state electron transfer of about 0.06 e⁻. Such a small effect must be considered with care, certainly by taking into account that the chemical shifts are also sensitive to changes of the local molecular environment in the complex such as a different molecular packing.[12,50] In addition, strong and asymmetric electron-withdrawing effects already operate on the TNF core from the NO_2 substituents. For instance, C_{12} is strongly positively charged by its withdrawing substituent, and

there is a difference of 12.5 ppm between carbon C_{11} and C_{13} in pristine TNF, which is the result of the symmetry breaking by the electron-withdrawing NO_2 group attached to carbon C_4.

A clear conclusion on the juxtaposition of TNF can be drawn from the 2D $^1\text{H}-^{13}\text{C}$ heterocorrelation NMR measurements. The signals indicated with red arrows in Figure 6 result from coherence transfer between the HAT6 tail proton spins H_2-H_6 and specific TNF carbons labeled in the inset. The presence of these $^1\text{H}-^{13}\text{C}$ correlation signals requires a close spatial proximity of protons and carbons that are involved. It has been shown that the time-oscillatory magnetization buildup of $^1\text{H}-^{13}\text{C}$ heteronuclear CP-MAS spectra can be related to the dipolar coupling strength, and therefore the internuclear distances, between the involved spin pairs.[53,54] From the mixing time corresponding with the maximum CP intensity, which appears to be around 10 ms (see also Figure S7), we estimate that the cross-polarized TNF carbons should be within an approximate distance of 0.6 nm from the HAT6 tail protons. Thus, the TNF should be, at least for the major part, within the tail region of the HAT6 molecules. On the other hand, no interaction between TNF and the core of HAT6 was observed. The proton H_{core} attached to the HAT6 core only shows cross-polarization with HAT6 carbons (Figure 6). Note that the signals marked with yellow arrows are due to the imperfect deuteration of TNF, since their intensity evolution as a function of mixing time (Figure S7) is comparable to protonated TNF and their chemical shift in the ^1H dimension matches with the involved TNF protons. For the differently deuterated sample, HAT6d-TNF, very little coherence transfer between TNF protons and any of the HAT6 carbons was observed. The absence of a significant reverse CP from TNF to the HAT6 tails is likely due to the different number of protons involved (12 for HAT6 tail protons H_2-H_5, 1 for TNF protons).

Finally, we consider some observations that relate to the dynamics of the liquid crystalline samples. First, the CP buildup of the carbons at the end of the aliphatic side chains is much slower than for ^{13}C nuclei close to the aromatic core of HAT6 (see Supporting Information). For both HAT6 and HAT6-TNF, the CP rate decreases from carbon C_2 to C_6, this being consistent with an increased dynamics along the aliphatic tails. Liquid-like motions due to "flip-flopping" of the dihedral angles between the carbons of the HAT6 tails occur on a comparable

time scale for the CT complex and for pristine HAT6.[17,31] Second, a rapid buildup of spin polarization is observed for the core $^{13}C_H$ (within 0.1 ms for both HAT6 and HAT6-TNF at ambient temperature) and for the TNF C−H carbons (within 1 ms), revealing a more rigid environment than for the tails. Third, the resolution in the proton dimension (e.g., Figure 6) for all HAT6 and TNF signals is quite good for the solid state MAS data sets collected without homonuclear decoupling during t_1 (^1H) evolution.[39] This narrowing of the ^1H line widths implies that the dipolar coupling in the liquid crystalline samples is partially averaged. The combination of a rapid rigid-like CP buildup and the narrowing of the ^1H line widths are indicative of selective averaging or quenching of weak longer range homonuclear $^1H−^1H$ dipolar interactions by anisotropic motion of the HAT6 and TNF molecules in the liquid crystalline phase. Indeed, we already found that in the liquid crystalline phase the HAT6 molecules are subject to small anisotropic translational (<0.1 nm) and rotational (a few degrees) molecular motions on the picosecond time scale.[31] In addition, in the CT complex these thermal motions of HAT6 are slowed down by a factor of about 2, while the anisotropic motions of the TNF molecules are faster than for the HAT6.[17] Larger molecular displacements of HAT6, related to dynamic defects in the liquid crystalline phase,[31] occur on time scales up to milliseconds.[47,55] These motions can quench the long-range dipolar interactions and contribute to the narrowing of the ^1H lines in the data sets without decoupling, while allowing at the same time for the high CP rates for the ^{13}C in the aromatic core by strong short-range heteronuclear dipolar interactions.

■ DISCUSSION

The morphologies of liquid crystalline CT complexes have been under debate for many years.[14,17,19−25] Several experimental approaches have been used to resolve their structure, including absorption spectroscopy, dielectric relaxation spectroscopy, NMR, but mostly diffraction techniques. The majority of experiments were qualitatively translated into a structural model, giving rise to entirely different propositions for the morphology of the CT complex. In contrast, pure DLC phases were successfully analyzed by using classical molecular dynamics (MD) simulations to bridge the gap between experiment and structural model.[31,56,57] However, such an approach faces many difficulties for donor−acceptor systems, including a proper description of the delocalized nature of the charge distribution in the complex. Therefore, we included the force field more indirectly via the energy penalty term in the refinement of the HAT6-TNF diffraction patterns. Despite this sophisticated method, the diffraction analyses alone did not resolve, but rather underlined, the controversy in the literature. This is somewhat surprising, since one would expect the two models to show different scattering intensities from the intra- and intercolumnar planes. It turns out that the liquid crystalline phase, with such large molecules and abundant averaging motions, is too complex for the limited information content of their diffraction patterns. Nevertheless, there are some observations in the diffraction that lean toward the intercolumnar model. In the sandwich arrangement, a close packing of the columns is needed to match their spacings with the observed reflections. This results in a density (1.14 g cm$^{−3}$) deviating slightly, but significantly, from the observed value for HAT6d-TNFd (1.08 ± 0.01 g cm$^{−3}$). Another consequence is the large disorder in TNF positions within the column due to the positional frustration of alternating TNF and HAT6

positions on the hexagonal lattice, making such model less likely on spatial considerations (Figure 4). For the intercolumn model the density (1.10 g cm$^{−3}$) is closer to the observed value, and the reproduction of small reflections in the diffraction pattern appears slightly better than for the sandwich model. Furthermore, as stated above, in a sandwich configuration one would expect a significant [001/2] superstructure reflection due to the repeating dimer unit, which appears to be absent in both the measured orientation-dependent XRD[17] and neutron diffraction patterns, while at the same time a strong [001] reflection is observed.

A clearer conclusion on the CT-complex morphology can be drawn when the results extracted from 2D NMR are also considered. The observed polarization transfer between the tails of HAT6 and almost all carbons of TNF requires that the major fraction of the TNF molecules lies between the aliphatic tails of HAT6. This arrangement appears only possible for the intercolumnar juxtaposition of TNF and also supports the vertical orientation of TNF from the diffraction analyses. In the vertical orientation, most of the TNF carbons are separated from HAT6 tail hydrogen atoms by about 0.3−0.7 nm. This separation is consistent with the estimated $^1H−^{13}C$ transfer range of 0.6 nm obtained from the cross-polarization transfer kinetics between the tail hydrogens and TNF carbons. In the alternative arrangement with TNF sandwiched within the HAT6 column, the TNF molecules only partly enter the tail region of HAT6 (Figure 4). With this arrangement the distances from the TNF carbons to the HAT6 tail hydrogen atoms are typically larger than 0.6 nm, which is too large to account for the observed correlations with the HAT6 tails. In addition, cross-polarization between TNF protons and the HAT6 core should be facilitated by such a sandwich arrangement and is not observed.

The NMR analyses also seem to indicate that charge transfer from the HAT6 core to TNF already takes place in the ground state of the complex. The effect would however be rather small: the chemical shift changes on HAT6 in the CT complex correspond to a ground state charge transfer of about 0.06 electron. Therefore, we will further investigate the existence of such a delocalization of the electron density in a forthcoming publication. In any event, excited state or ground state charge transfer from the HAT6 core to TNF requires that the electron acceptor should not be too far from the aromatic core. For the intercolumnar CT-complex structure the diffraction analyses resulted in HAT6core-TNF distances of 4−10 Å, mostly involving the optically active NO_2 groups of TNF. To ensure a sufficient orbital overlap for CT electron delocalization, most of the TNF molecules should be in the lower part of this range.

Clearly, the consistent analysis reveals a CT-complex morphology with dynamically disordered TNF molecules that are vertically oriented between the HAT6 columns, i.e., within the aliphatic tail region. What does this mean for photovoltaic applications? A promising observation is that there is a hole conducting column present that is well separated from the electron acceptors. The columnar morphology has changed drastically in the composites, with a time-averaged tilted orientation and smaller average distances between the neighboring HAT6 molecules within the column (0.34 nm) than in neat HAT6 (0.36 nm). In the CT complex the hole transport through the column will thus still be possible, while the CT process enables efficient charge separation. The liquid crystalline structure and its facile alignment over macroscopic distances is an important asset for device realization. For the

HAT6/TNF 1:1 material it is observed (Figure S8) that millimeter-long oriented domains can indeed be produced. Such domains would ideally connect the two current collectors in a PV device. For TNF it is clear that the vertical and disordered orientation does not favor long-range electron transport. In the present configuration the TNF molecules act more as molecular traps for efficient electron transport, in line with experimental observations.[29,58] The future PV application of CT complexes such as HAT6-TNF thus relies on improving the electron transport channel (Figure 7). For instance, by
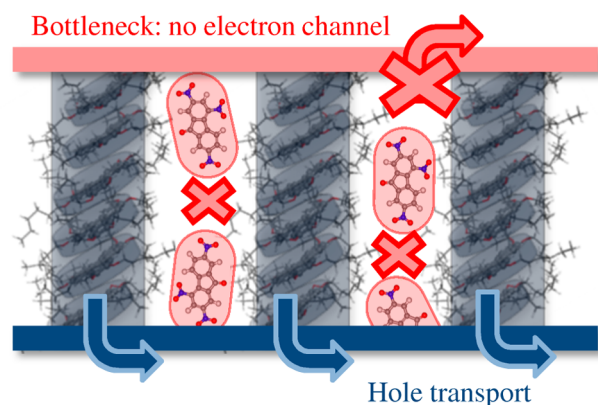

Figure 7. Illustration of a HAT6-TNF bulk-heterojunction PV device with self-assembled columns at the molecular nanoscale.

searching for better acceptors that self-assemble into a separate channel, designing molecularly connected donor and acceptor groups[3] or by investigating alternative device architectures such as those in the field of biomimetic solar cells.[59,60]

CONCLUSIONS

We have elucidated the complex morphology of the prototypic DLC charge-transfer compound HAT6-TNF by combining density measurements, detailed neutron diffraction studies, and sophisticated NMR techniques. We found that the liquid crystalline HAT6 columns are still present in the CT compound, although the neighboring molecules are slid laterally leading to a tilted column. The TNF molecules are dynamically disordered with a predominant vertical orientation between the HAT6 columns, in the region of the liquid like moving aliphatic tails. NMR proton line widths and cross-polarization rates are consistent with previously observed anisotropic "wobbling" motions of the HAT6 and TNF molecules on the picosecond time scale. The data can be reconciled with minor partial charge transfer from the HAT6 core to the electron accepting TNF in the ground state. The persistence of the hole conducting HAT6 column in the CT complex is promising for future application in organic PV systems.

ASSOCIATED CONTENT

ⓢ Supporting Information

Further details on the simulated diffraction patterns of oriented HAT6-TNF samples, the assignment of the NMR spectra, and macroscopic alignment of the discotic CT compounds. This material is available free of charge via the Internet at http://pubs.acs.org.

AUTHOR INFORMATION

Corresponding Author
*E-mail F.M.Mulder@tudelft.nl.
Notes
The authors declare no competing financial interest.

ACKNOWLEDGMENTS

REFERENCES

(1) Kaafarani, B. R. *Chem. Mater.* **2011**, *23*, 378−396.
(2) Wong, W. W.; Ma, C. Q.; Pisula, W.; Yan, C.; Feng, X.; Jones, D. J.; Muellen, K.; Janssen, R. A.; Baeuerle, P.; Holmes, A. B. *Chem. Mater.* **2010**, *22*, 457−466.
(3) Yamamoto, Y.; Fukushima, T.; Suna, Y.; Ishii, N.; Saeki, A.; Seki, S.; Tagawa, S.; Taniguchi, M.; Kawai, T.; Aida, T. *Science* **2006**, *314*, 1761−1764.
(4) Schmidt-Mende, L.; Fechtenkotter, A.; Mullen, K.; Moons, E.; Friend, R. H.; MacKenzie. *Science* **2001**, *293*, 1119−1122.
(5) Van de Craats, A. M.; Warman, J. M.; Fechtenkotter, A.; Brand, J. D.; Harbison, M. A.; Mullen, K. *Adv. Mater.* **1999**, *11*, 1469−1472.
(6) Sergeyev, S.; Pisula, W.; Geerts, Y. H. *Chem. Soc. Rev.* **2007**, *36*, 1902−1929.
(7) Gunes, S.; Neugebauer, H.; Sariciftci, N. S. *Chem. Rev.* **2007**, *107*, 1324−1338.
(8) Thompson, B. C.; Frechet, J. M. J. *Angew. Chem., Int. Ed.* **2008**, *47*, 58−77.
(9) Helgesen, M.; Sondergaard, R.; Krebs, F. C. *J. Mater. Chem.* **2010**, *20*, 36−60.
(10) Mayer, A. C.; Scully, S. R.; Hardin, B. E.; Rowell, M. W.; McGehee, M. D. *Mater. Today* **2007**, *10*, 28−33.
(11) Li, J. J.; He, Z. Q.; Zhao, H.; Gopee, H.; Kong, X. F.; Xu, M.; An, X. X.; Jing, X. P.; Cammidge, A. N. *Pure Appl. Chem.* **2010**, *82*, 1993−2003.
(12) Percec, V.; Glodde, M.; Bera, T. K.; Miura, Y.; Shiyanovskaya, I.; Singer, K. D.; Balagurusamy, V. S. K.; Heiney, P. A.; Schnell, I.; Rapp, A.; Spiess, H. W.; Hudson, S. D.; Duan, H. *Nature* **2002**, *419*, 384−387.
(13) Hirose, T.; Yumoto, T.; Matsumoto, K.; Mitsushio, S.; Kawakami, O.; Yasutake, M. *Mol. Cryst. Liq. Cryst.* **2010**, *524*, 68−101.
(14) Markovitsi, D.; Bengs, H.; Ringsdorf, H. *J. Chem. Soc., Faraday Trans.* **1992**, *88*, 1275−1279.
(15) Blann, W. G.; Fyfe, C. A.; Lyerla, J. R.; Yannoni, C. S. *J. Am. Chem. Soc.* **1981**, *103*, 4030−4033.
(16) Mulliken, R. S. *J. Phys. Chem.* **1952**, *56*, 801−822.
(17) Kruglova, O.; Mencles, E.; Yildirim, Z.; Wubbenhorst, M.; Mulder, F. M.; Stride, J. A.; Picken, S. J.; Kearley, G. J. *ChemPhysChem* **2007**, *8*, 1338−1344.
(18) Boden, N.; Bushby, R. J.; Lozman, O. R. *Mol. Cryst. Liq. Cryst.* **2004**, *411*, 1387−1396.
(19) Praefcke, K.; Holbrey, J. D. *J. Inclusion Phenom. Mol. Recognit. Chem.* **1996**, *24*, 19−41.
(20) Kamikawa, Y.; Kato, T. *Org. Lett.* **2006**, *8*, 2463−2466.
(21) Percec, V.; Imam, M. R.; Peterca, M.; Wilson, D. A.; Graf, R.; Spiess, H. W.; Balagurusamy, V. S. K.; Heiney, P. A. *J. Am. Chem. Soc.* **2009**, *131*, 7662−7677.
(22) Ringsdorf, H.; Wustefeld, R.; Zerta, E.; Ebert, M.; Wendorff, J. H. *Angew. Chem., Int. Ed. Engl.* **1989**, *28*, 914−918.
(23) Vaughan, G. B. M.; Heiney, P. A.; Mccauley, J. P.; Smith, A. B. *Phys. Rev. B* **1992**, *46*, 2787−2791.

(24) Davidson, P.; Levelut, A. M.; Strzelecka, H.; Gionis, V. *J. Phys., Lett.* **1983**, *44*, L823−L828.

(25) Kouwer, P. H. J.; Jager, W. F.; Mijs, W. J.; Picken, S. J. *Macromolecules* **2002**, *35*, 4322−4329.

(26) Beckers, E. H. A.; Meskers, S. C. J.; Schenning, A. P. H. J.; Chen, Z. J.; Wurthner, F.; Marsal, P.; Beljonne, D.; Cornil, J.; Janssen, R. A. J. *J. Am. Chem. Soc.* **2006**, *128*, 649−657.

(27) Boden, N.; Bushby, R. J.; Clements, J.; Luo, R. *J. Mater. Chem.* **1995**, *5*, 1741−1748.

(28) Kumar, P. S.; Kumar, S.; Lakshminarayanan, V. *J. Phys. Chem. B* **2008**, *112*, 4865−4869.

(29) Donovan, K. J.; Scott, K.; Somerton, M.; Preece, J.; Manickam, M. *Chem. Phys.* **2006**, *322*, 471−476.

(30) Markovitsi, D.; Marguet, S.; Bondkowski, J.; Kumar, S. *J. Phys. Chem. B* **2001**, *105*, 1299−1306.

(31) Haverkate, L. A.; Zbiri, M.; Johnson, M. R.; Deme, B.; Mulder, F. M.; Kearley, G. J. *J. Phys. Chem. B* **2011**, *115*, 13809−13816.

(32) Kruglova, O.; Mulder, F. M.; Kotlewski, A.; Picken, S. J.; Parker, S.; Johnson, M. R.; Kearley, G. J. *Chem. Phys.* **2006**, *330*, 360−364.

(33) Haverkate, L. A.; Zbiri, M.; Johnson, M. R.; Deme, B.; Mulder, F. M.; Kearley, G. J. *J. Phys. Chem. B* **2012**, *116*, 3908.

(34) Sun, H.; Rigby, D. *Spectrochim. Acta, Part A* **1997**, *53*, 1301−1323.

(35) Rigby, D.; Sun, H.; Eichinger, B. E. *Polym. Int.* **1997**, *44*, 311−330.

(36) McQuaid, M. J.; Sun, H.; Rigby, D. *J. Comput. Chem.* **2004**, *25*, 61−71.

(37) Brooks, C. L.; Pettitt, B. M.; Karplus, M. *J. Chem. Phys.* **1985**, *83*, 5897−5908.

(38) McQuarrie, D. A. *Statistical Mechanics*; Harper & Row: New York, 1976; Chapter 3.

(39) vanRossum, B. J.; Boender, G. J.; deGroot, H. J. M. *J. Magn. Reson., Ser. A* **1996**, *120*, 274−277.

(40) Metz, G.; Wu, X. L.; Smith, S. O. *J. Magn. Reson., Ser. A* **1994**, *110*, 219−227.

(41) Bennett, A. E.; Rienstra, C. M.; Auger, M.; Lakshmi, K. V.; Griffin, R. G. *J. Chem. Phys.* **1995**, *103*, 6951−6958.

(42) Pisula, W.; Kastler, M.; Wasserfallen, D.; Robertson, J. W. F.; Nolde, F.; Kohl, C.; Mullen, K. *Angew. Chem., Int. Ed.* **2006**, *45*, 819−823.

(43) Bushby, R. J.; Boden, N.; Kilner, C. A.; Lozman, O. R.; Lu, Z. B.; Liu, Q. Y.; Thornton-Pett, M. A. *J. Mater. Chem.* **2003**, *13*, 470−474.

(44) Rutar, V.; Blinc, R.; Vilfan, M.; Zann, A.; Dubois, J. C. *J. Phys. (Paris)* **1982**, *43*, 761−765.

(45) Dvinskikh, S. V.; Sandstrom, D.; Zimmermann, H.; Maliniak, A. *Prog. Nucl. Magn. Reson. Spectrosc.* **2006**, *48*, 85−107.

(46) Brown, S. P.; Schnell, I.; Brand, J. D.; Mullen, K.; Spiess, H. W. *J. Mol. Struct.* **2000**, *521*, 179−195.

(47) Shen, X.; Dong, R. Y.; Boden, N.; Bushby, R. J.; Martin, P. S.; Wood, A. *J. Chem. Phys.* **1998**, *108*, 4324−4332.

(48) Natansohn, A. *Polym. Bull.* **1989**, *21*, 217−220.

(49) Natansohn, A. *Macromolecules* **1991**, *24*, 1662−1669.

(50) Simmons, A.; Natansohn. *Macromolecules* **1991**, *24*, 3651−3661.

(51) Zbiri, M.; Johnson, M. R.; Kearley, G. J.; Mulder, F. M. *Theor. Chem. Acc.* **2010**, *125*, 445−451.

(52) Lemaur, V.; Da Silva Filho, D. A.; Coropceanu, V.; Lehmann, M.; Geerts, Y.; Piris, J.; Debije, M. G.; Van de Craats, A. M.; Senthilkumar, K.; Siebbeles, L. D. A.; Warman, J. M.; Bredas, J. L.; Cornil, J. *J. Am. Chem. Soc.* **2004**, *126*, 3271−3279.

(53) van Rossum, B. J.; de Groot, C. P.; Ladizhansky, V.; Vega, S.; de Groot, H. J. M. *J. Am. Chem. Soc.* **2000**, *122*, 3465−3472.

(54) van Rossum, B. J.; van Liemt, W. B. S.; Gast, P.; Lugtenburg, J.; de Groot, H. J. M. *Appl. Magn. Reson.* **2007**, *31*, 145−158.

(55) Stevensson, B.; Marini, A.; Zimmermann, H.; Maliniak, A. *J. Phys. Chem. B* **2011**, *115*, 7561−7567.

(56) Andrienko, D.; Kirkpatrick, J.; Marcon, V.; Nelson, J.; Kremer, K. *Phys. Status Solidi B* **2008**, *245*, 830−834.

(57) Feng, X. L.; Marcon, V.; Pisula, W.; Hansen, M. R.; Kirkpatrick, J.; Grozema, F.; Andrienko, D.; Kremer, K.; Mullen, K. *Nat. Mater.* **2009**, *8*, 421−426.

(58) Markovitsi, D.; Germain, A.; Millie, P.; Lecuyer, P.; Gallos, L. K.; Argyrakis, P.; Bengs, H.; Ringsdorf, H. *J. Phys. Chem.* **1995**, *99*, 1005−1017.

(59) Pandit, A.; de Groot, H. J. M. *Photosynth. Res.* **2012**, *111*, 219−226.

(60) Katterle, M.; Prokhorenko, V. I.; Holzwarth, A. R.; Jesorka, A. *Chem. Phys. Lett.* **2007**, *447*, 284−288.